



UNIVERSITY OF AMSTERDAM



MSc Physics and Astronomy
Track: Astronomy & Astrophysics

Master Thesis

Modelling the time lags in Black Hole X-Ray binaries

by

Dani van Enk
11823526 (UVA)

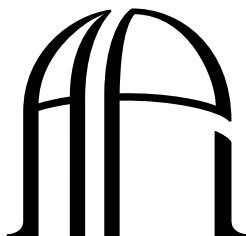
July 31, 2023

60 ECTS

June 2021 - July 2023

Supervisors:
dr. Phil Uttley
dr. Phil Uttley

Examiners
dr. Phil Uttley
prof. dr. Sera Markoff



ANTON PANNEKOEK
INSTITUTE

Contents

1	Introduction	1
1.1	Black Hole History	1
1.2	Types of Black Holes	2
1.3	X-ray Binaries	2
1.4	X-ray Detection	3
1.5	X-ray spectrum	5
1.6	Accretion States	7
1.7	Variabilities	9
1.8	Previous Models	11
1.9	Thesis overview	12
2	Model	14
2.1	Effects of Corona emissions	15
3	Results	17
3.1	Tests	17
3.2	Fits	17
4	Conclusion	19
A	Code	24

Chapter 1

Introduction

Ever since their conception, black holes have been objects filled with mystery. Them being patches of space where nothing would be able to escape makes them really hard to be seen. The only way that black holes can be detected  is in an indirect way, in other words via matter  objects being affected by its gravitational pull. This makes them incredibly hard  to detect, let alone study. Luckily in recent decades, this has become easier with different and new techniques to study these mysterious objects.

1.1 Black Hole History

A few years after Albert Einstein came up with the idea of the general theory of relativity  Karl Schwarzschild came up with the first modern solution to the general relativity theory that characterizes a black hole ([Schwarzschild 1916](#)). It would still take decades before "black holes" would be interpreted as a region of space that nothing can escape from in a paper by David Finkelstein ([Finkelstein 1958](#)). However, the idea of a "black hole" remained a mathematical curiosity. It took until the discovery of a neutron star in 1967 ([Hewish et al. 1968](#)) for interest in gravitationally collapsed compact objects to increase. Just 5 years before that proof of X-ray sources outside our solar system had been found ([Giacconi et al. 1962](#)) which prompted the launch of a mission into space to look for X-ray sources.  this mission, several X-ray sources were observed, including Cygnus X-1. However, the observations showed that Cygnus X-1 had fluctuations in the X-ray of several times a second. Just a year later two different radio observatories independently located a star (HDE 226868) that was thought to be the source  of the X-ray radiation. However, since it was found to be a super-giant star  can't generate X-rays on its own. So it needed to have a companion that could heat up the hot gas to a high enough temperature to generate those X-rays ([Kristian et al. 1971; Braes & Miley 1971](#)). Then in 1972

this companion, the first Black Hole, was detected and identified independently by multiple researchers ([Webster & Murdin 1972](#); [Bolton 1972](#)). It would still take until the following year for there to be consensus about it being a black hole. Researchers found fluctuations in the X-ray signal that could point to mass fluctuations in an accretion disk this combined with the fact that it can't be a neutron star due to its mass made them quite certain that Cygnus X-1 is a black hole ([Rothschild et al. 1974](#); [Shipman 1975](#)).

1.2 Types of Black Holes



The current understanding of black holes is that there are generally 3 types of black holes. The most massive of black holes are called supermassive black holes, these black holes lie in the centers of galaxies ([Kormendy & Richstone 1995](#)) and due to their mass ranging from hundreds of thousands to several billions of solar masses (M_{\odot}) are they believed to be one of the driving forces that keep a galaxy together. They are thought to have formed in the early universe. Secondly, a smaller type of black hole is the intermediate-mass black hole. These have masses from hundreds to hundreds of thousands of solar masses. They have first been proposed by [Colbert & Mushotzky \(1999\)](#), but it took till recently with the detection of gravitational waves for intermediate-mass black holes to be detected ([Abbott et al. 2020](#)). Finally, the black holes we know the most of are stellar-mass black holes. These black holes are formed when a big enough star collapses after going supernova ([Celotti et al. 1999](#)), creating a black hole from about five to tens of solar masses. For this thesis, the focus is on the last type.

1.3 X-ray Binaries

As mentioned in [Boss & Keiser \(2014\)](#) a large proportion of stars in the galactic neighborhood are believed to be multi-star systems. In the case of 2 components, these are called binaries. If one of the components in the binary goes supernova it can create a neutron star or black hole. In this case, such kind of binary systems are called X-ray binaries or XRBs in short. The other star in the system can as it lives through its life start accreting material onto the compact object, first modeled by [Shakura & Sunyaev \(1973\)](#). This accretion generates X-rays as the material falls in towards the compact object. XRBs can be separated into several different major categories which tell something about the type of donor star.

First are the High-mass X-ray binaries (HMXB), where the donor is a massive star. This usually is an O or B star, a blue giant star sometimes even a red supergiant or Wolf-Rayet star. These stars have strong stellar winds ([Höfner et al. 2003](#); [Sandin & Höfner 2003, 2004](#); [Mattsson & Höfner 2011](#)) which get partially captured by the

compact object. This causes the material of the stellar wind to accrete onto the compact object.

The next type is a Low-mass X-ray binary (LMXB), where the donor star is a  in sequence star, red giant, or white dwarf. In these kinds of binaries, the donor star over the course of its life starts to fill its Roche lobe. As it reaches the edge of the Roche lobe it will start to enter into the Roche lobe of the compact object, accreting onto it.

Finally, there's a type between both which is called an Intermediate-mass X-ray binary (IMXB), in which the donor star is an intermediate-mass star ([Tauris et al. 2000](#); [Podsiadlowski et al. 2002](#)).

1.4 X-ray Detection

 The X-ray that is emitted by this accretion disk  can tell us a lot about what is happening inside the accretion disk. One way to shed more light on this is to use X-ray telescopes to study the physics behind these emissions.

One such telescope is NASA's Neutron Star Interior Composition Explorer or NICER for short which is located on the International Space Station (ISS) shown in figure [1.1](#). It was launched and installed on the ISS in 2017 as part of the Explorer Program. With its X-ray Timing Instrument with an array of 56 X-ray detectors, it is able to detect photons in the range of 0.2 keV - 12 keV. Using GPS, NICER is able to flag the timestamp of photons detected with a precision that is less than 300 ns as well as their energy ([Gendreau et al. 2012](#)). As its name suggests NICER was initially launched to study the interior composition of neutron stars. However, due to the very sensitive nature of its instruments, it was the perfect solution for detecting other X-ray sources as well like XRBs.

A different but older telescope is ESA's X-ray Multi-Mirror Mission or XMM-Newton telescope. Unfortunately, unlike  with NICER, no images exist of its current state. There are some computer-generated images of what it would look like and a replica exists located in Cite de l'espace in Toulouse as shown in figure [1.2](#). It was launched in 1999 as part of the Horizon 2000 program. Its range of detection is 0.1 keV - 12 keV ([Wilson 2005](#)) which is fairly similar to NICER's range. However, XMM-Newton has 3 different types of instruments with fewer detectors than NICER. Its first type of instrument is the European Photon Imaging Camera (EPIC) of which it has 3. 2 of those are of the type MOS-CCD for soft photon detection (up to 5-10 keV) which have 7 detectors. The  detectors have a readout cycle of around 2.9 seconds ([Turner et al. 2001](#)). The other EPIC is dedicated to hard photon detection ( than 5-10 keV) which has 12 detectors of the pn-CCD type. The hard photon EPIC is much faster than the MOS-CCD at an impressive 80 ms readout speed, which in a special mode can be brought down to 40 ms ([Strüder et al. 2001](#)). Its





FIG. 1.1 – Picture shown of NICER as mounted on the ISS. One of the solar panels can be seen behind the telescope and on the telescope itself, its 56 X-ray detectors.

Source: https://svs.gsfc.nasa.gov/12854#media_group_9204



FIG. 1.2 – Picture shown of a replica of the XMM-Newton telescope in Cite de l'Espace in Toulouse.

Source: https://it.wikipedia.org/wiki/File:XMM-Newton_at_Cite_de_l%27espace_4.jpg

second type of instrument is the Reflection Grating Spectrometer (RGS) which is a grating spectrometer consisting of 2 9 MOS-CCD arrays to be able to detect elements present in the target. Finally, it also has an Optical Monitor (OM) system which is an optical/ultra-violet imaging system to allow for simultaneous observations with the X-ray systems.

1.5 X-ray spectrum

These telescopes are then used to study the X-rays that are emitted by the XRB. This generates an X-ray spectrum of the source which is composed of several different components as can be seen in figure 1.3 which is an edited version of figure 9 shown in [Gierliński et al. \(1999\)](#). This is a spectrum for the black hole Cygnus-X1. This thesis will focus on such black hole XRBs. While the physics at play near the outside of the disk are fairly well known the inner hot parts of the disk close to the black hole are much less well known. Looking at the object in X-ray will uncover some of this as the inner parts of the system are the source of the X-ray emissions.

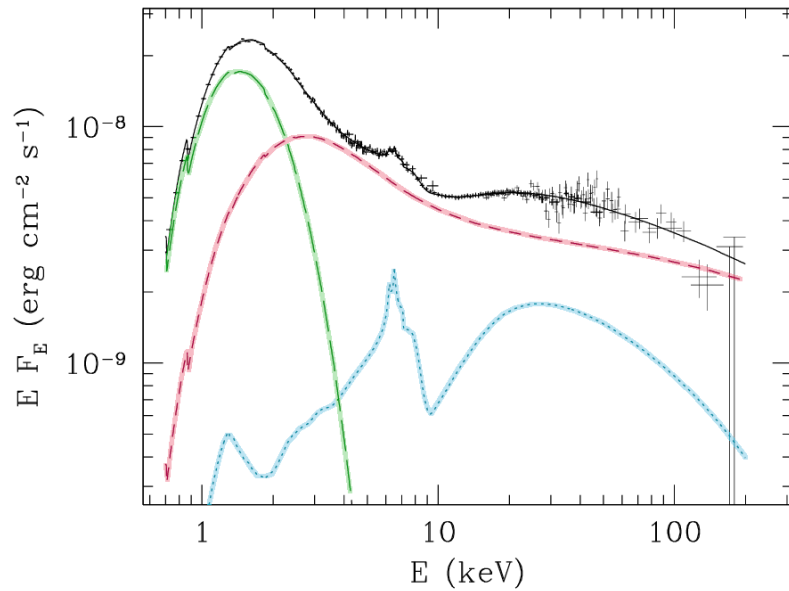


FIG. 1.3 – Shows X-ray spectrum of Cygnus-X1 as shown in [Gierliński et al. \(1999\)](#) figure 9. Also shown in this figure are the separate components of the X-ray spectrum. The green dashed line shows the black body radiation component of the disk, the pink dashed line is the Comptonization power law of the corona, and the blue dotted line is the reflection and reproduced photons from the corona to the disk.

 The material that is caught by the gravitational field of the black hole gravitates towards a disk around the black hole. As the material is captured by the black hole

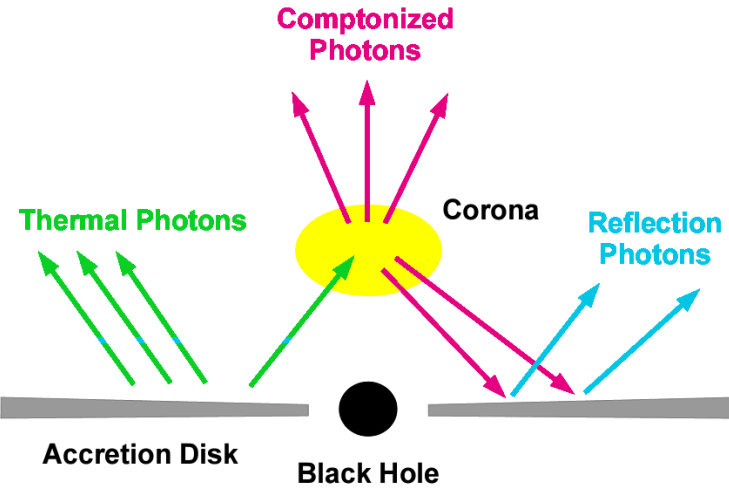


FIG. 1.4 – In this figure a schematic overview of emissions and how the flow through the system as a side-on slice. It is taken from Bambi (2021) figure 1 with altered colors to match figure 1.3. The scale nor position/shape of the corona is a true visualization of the nature of the system, it is shown this way for the sake of explanation. In green the Thermal black body emissions are shown from the accretion disk. In yellow a possible location and shape of the corona is shown. As the black body emissions get to the corona they get inversely Compton upscattered and emitted away from the corona, shown in pink. The coronal emissions are then reflected or reprocessed in the disk as shown in blue.

it all moves in the same direction around the black hole it experiences friction which causes the speed the material has in the normal direction to the spin of the black hole to go towards zero creating a flat disk around the black hole. However, due to the conservation of angular momentum, the material ends up orbiting the black hole in its respective circular orbits according to their angular momentum as that is the type of orbit with the least energy. This friction together with the magnetic shear caused by the Magnetorotational Instability generates viscous dissipation and turbulent flow in the disk which allows for angular momentum to be transported towards the outside of the disk and material to accrete onto the black hole (Balbus & Hawley 1991; Hawley & Balbus 1991, 1999; Balbus & Hawley 1992, 1998). This inward material flow generates a lot of thermal energy in the form of black body radiation as the material heats up as it gets closer to the black hole this causes the disk to become optically thick and geometrically thin (Shakura & Sunyaev 1973; Frank et al. 2002). As black body radiation is emitted at each radius which increases as the material gets closer to the black hole, this creates a multi-temperature black body emission as can be seen in figure 1.3 as the green dashed line. With the high temperatures in the inner parts of the disk (which can reach millions or billions of degrees) the emission is mainly in the Extreme Ultra-Violet or X-rays.

The black body X-rays that are emitted by the disk go in all directions, some of these are directed toward the black hole and the area around the black hole (shown in green in figure 1.4). This area is thought to be a hot optically thin cloud of electrons close to the black hole called a corona (shown in yellow in figure 1.4). These photons are high-energy X-ray photons originating from hot plasma ($\sim 10^8\text{-}10^9\text{K}$) (Shapiro et al. 1976), these are usually referred to "seed" photons as they are the seed for the Comptonization in the corona. As these "seed" photons from the disk enter this cloud they can get Inversely Compton up-scattered to (much) higher energies generating a power-law spectrum with a cut-off at higher energies as can be seen in figure 1.3 as the pink dashed line. However, much about the corona is not known. One of these is the exact shape or geometry of the corona. Some examples of proposals for this geometry are a thin blanket over the disk close to the black as proposed in Zdziarski et al. (2021), a hot flow region between the black hole and the disk (Rapisarda et al. 2016) or even a region at the base of an astrophysical jet as described in Markoff et al. (2005). The actual geometry of the corona could be something completely different or even a combination of the proposed shapes.

As the photons get up-scattered in the corona they go in all kinds of directions again just like with the disk emission (shown in figure 1.4 in pink). This time some photons reach back to the disk (Done et al. 2007) where they either get back-scattered reflecting off the disk, which creates a hump of high-energy up-scattered photons. Some of the photons have the right energy for certain line transitions in atoms that appear in the X-ray, a famous example of this is the K α -iron line. This reflection and reprocessing of the photons is usually classified as the reflection spectrum component of the X-ray spectrum and is shown in figure 1.3 as the blue dotted line and in blue in figure 1.4.

1.6 Accretion States

Most of the time, XRBs have been observed to be very quiet in the X-ray. However, X-ray spectrum and brightness alter a lot over different timescales. During these moments the disk is in quiescence and is relatively cold. On timescales of years can black holes exhibit drastic increases in X-ray emission that last weeks or months, called outbursts. It has been theorized that in the disk Hydrogen Ionisation can occur causing these outbursts (Dubus et al. 2001). At the beginning of such an outburst, the disk is about 10^4K which is very close to the ionization temperature of hydrogen. As such the disk mainly consists of neutral hydrogen. However, when the temperature rises due to for example turbulent motion. This causes the hydrogen in the disk starts ionizing, increasing the opacity of that part of the disk. As a result, the photons from that part of the disk get somewhat trapped raising the temperature, which causes more hydrogen to ionize. This creates a runaway process of ionization of the hydrogen is almost all fully ionized. This local heating causes the accretion

flow to increase which affects the neighboring radii making this heat wave propagate through the disk towards the black hole. This process makes the emission of the disk drastically increase in luminosity and is the start of the outburst (Frank et al. 2002; Done et al. 2007).



This increased accretion rate eventually gets bigger than the accretion rate of the donor star. As a result and both the temperature and pressure decrease, which consequently causes the same runaway process but in reverse. This continues until the disk returns to its quiescence state finishing the outburst. Even though this effect starts off locally, the changes in mass accretion cause different regions in the mass flow to be linked together (Frank et al. 2002; Done et al. 2007). However, unfortunately, this model is not yet fully complete and only gives part of the picture. Although in recent years it has been theorized that magnetic fields in the disk play an important role in the outburst process in the disk (Begelman et al. 2015).

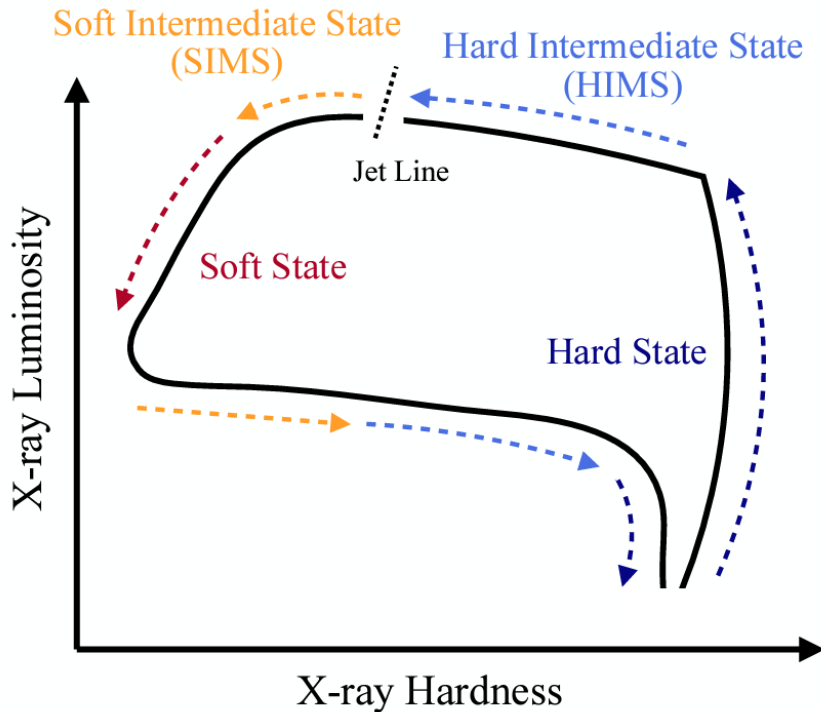


FIG. 1.5 – In this figure the evolution of an outburst is shown as it moves through the hardness (X-ray emission energy) and intensity plane (fetched from Wang et al. (2022) figure 1). The different accretion states are annotated in color as well as the corresponding direction arrow. The hard state is shown in dark blue, the hard intermediate state is shown in blue, the soft intermediate state is shown in yellow, and the soft state is shown in red.

Let's look at this process in more detail. As a black hole accretion disk goes through this outburst cycle it cycles through several different accretion states. These can be shown in a hardness-intensity diagram like shown in figure 1.5 (figure 1 in Wang et al.

(2022)), the hardness meaning the energy of the emitted photons, and the intensity relating to the total brightness luminosity of the disk. The hardness is the ratio between the earlier defined hard high energy to soft low energy photons as mentioned in section 1.4.

As mentioned before it starts out in a cold and quiescence. In this state, all called the hard state (HS), the corona gives the most emission compared to the disk. As such while the luminosity might be low the hardness of the photons that do get emitted is in the hard spectrum. In this state, the outflow is believed to be emitting photons in the radio regime, also known as the X-ray/radio correlation (Koljonen & Russell 2019). Over the course of a couple of weeks, the system starts to rise in luminosity as the hydrogen ionizes and the accretion rate increases.

The system then transitions into the next state the disk starts to heat up and generate more X-rays compared to radio emissions. In this Hard Intermediate State (HIMS) the hardness of the system starts to shift towards the "soft" regime. As this runaway process continues it continues to soften its hardness and gets into the Soft Intermediate State (SIMS). It has been found that in XRBs there's a strong coupling between ejection and accretion (Fender et al. 2004, 2009). While in the hard state, a compact and slightly relativistic jet is always present (Dhawan et al. 2000). Somewhere between the SIMS and HIMS states it quenches and transitions into a highly relativistic, discrete, and ballistic jet (Bright et al. 2020). The boundary between these two jet states is called the "jet line".

The system eventually locally depletes and the accretion rate starts to drop. As a result, the luminosity drops and the system has reached the soft state (SS). As mentioned before this causes the temperature to drop, causing the emission to harden because the disk emission moves back into the radio regime. The system goes through the SIMS and HIMS again and the highly relativistic, discrete, and ballistic jet transitions back into a compact jet but this is not well understood (Miller-Jones et al. 2012; Kalemci et al. 2013). Finally, it reaches the hard state again as the disk emissions have fully turned into radio emissions again and the luminosity drops drastically again.

It is important to distinguish between these states since, as mentioned above, they have very different accretion rates. Depending on the state either the corona (in the HS) or the disk (in the SS) are more dominant in the X-ray spectrum (Belloni & Motta 2016), or the type of jet between the two regimes on both sides of this "jet line".

1.7 Variabilities

Of course, as mentioned before the emissions of an XRB are not stationary in time. While the singular X-ray spectrum can already say quite a bit about what happens in the accretion disk and corona, to know more a time series of X-ray spectra should be observed. Analyzing these time series will give more insight into the physics



behind long and shot time-scale variabilities. One way to do this is by using Fourier transform techniques to convert the time series from the time domain to the frequency domain. This operation can bring any periodicity of the spectrum to light curves. When taking the Fourier product between two different energy bands the difference between those energy bands can be studied. The Fourier Product is taken between two time series of the same energy band and is called a power spectrum. This shows for each Fourier frequency the amplitude of the variability.

If the variability between two energy bands is to be studied Fourier techniques can also be used as is mentioned in great detail in [Uttley et al. \(2014\)](#). Some distinct energy bands are chosen and a cross-spectrum is calculated by using the Fourier product between the time series of both energy bands, this is also known as X-ray spectral timing. Using this cross-spectrum the coherence between the two light curves can be calculated.

What also can be calculated from this cross-spectrum is any phase difference or lag between the Fourier frequencies of each energy band. Since the result of a Fourier transform is a series of complex amplitudes for each Fourier frequency, this phase lag can be retrieved by taking the argument of the complex amplitude. This can then be converted into a temporal lag by dividing the found phase lag by $2\pi\nu_i$ where ν_i is the mean of the Fourier frequency used.

These time lags between the light curves of different energy bands have been observed in several different sources. Several different lags can be formulated when looking at different energy bands. These lags are dependent on several different aspects of the system like which energy band but also the accretion state & geometry/scale of the disk or corona. One of the first studied lags was the hard lags between different corona energy bands, as such they are called hard PL lags. Where in the hard state where high energy corona emissions start to lag behind lower energy corona emissions. These were first studied by missions such as Ginga and later Rossi X-ray Timing Explorer (RXTE) using data above 3 keV ([Miyamoto et al. 1988](#); [Nowak et al. 1999](#); [Grinberg et al. 2014](#); [Altamirano & Méndez 2015](#)), which were predecessors of XMM-Newton & NICER as mentioned in section [1.4](#).

Later the focus shifted towards more studies looking at softer bands of the black body disk emissions and the launches of telescopes with more sensitive equipment like XMM-Newton & Nicer (see section [1.4](#)). Using XMM-Newton data on GX-339-4, [Wilkinson & Uttley \(2009\)](#) found that its disk emission variabilities can change on timescales as quickly as less than seconds to several minutes. The variabilities are the strongest for variabilities on bigger than-second timescales. Later [Uttley et al. \(2011\)](#) found using the same data, that for Fourier frequencies smaller than 1 Hz the soft lags between the disk (0.5-0.9 keV) and the corona (2-3 keV) were several times bigger than between the different power-law energy bands at the same frequencies. For frequencies bigger than 1 Hz this flips around with the "soft" lags becoming negative lags of around 1-2 ms. This means the mass accretion fluctuations first arrive in the corona before the power-law emissions are varied. Which in turn illuminates the disk and part emissions are reprocessed in the disk. This generates

a soft "reverberation" X-ray signal that corresponds to the light-travel delays of tens of gravitational radii (Mastroserio et al. 2018; Mahmoud et al. 2019). This "reverberation" and its role in the production of short-term soft lags along with delays in the K- α line, the broadened iron line, at similar frequencies by NICER observations (Kara et al. 2019).

1.8 Previous Models

Over the years, several models have been crafted to explain both the behavior of the hard PL lags as well as the soft disk-PL lags.

In the case of the hard PL lags 2 possible origins have been proposed. The first origination assumes the corona to be a very extended corona. In this model, the seed photons being emitted from the disk get upscattered multiple times to higher energies in the corona leading to delays. These delays are directly linked to the light-travel times and thus can cause hard PL lags to approach milliseconds on tens of seconds time scales. The corona however would need to be extended very far up from the disk on the order of thousands of gravitational radii. Which in turn needs a lot of energy to fully heat a spherical corona of that size. Due to this, it is believed to be caused by an observed hard state jet (Reig et al. 2003; Giannios et al. 2004; Kylafis et al. 2008).

A different proposed model is one where these hard PL lags are instead likely to originate from the accretion flow itself on small timescales. This may even be the origin of the broadband noise variabilities that are detected (Lyubarskii 1997; Uttley et al. 2005). The disk is taken to be a truncated disk instead of a full disk with the corona consisting of a hot geometrically thick accretion flow that increases in temperature and thus hardens as it gets closer to the black hole (Kotov et al. 2001; Arévalo & Uttley 2006). With thought to be produced by the propagation delays between radii where high variability frequencies show a decrease for both soft and hard photons emissions as the matter gets closer and closer to the black hole. Through the years this model has gotten more complex to try and explain the variability of the power spectrum as well as the dependence of the lags on both the energy and frequency. Some of these attempts were by trying to introduce discontinuities for the emission spectrum (Rapisarda et al. 2016; Mahmoud & Done 2018b), input variability signal (Mahmoud & Done 2018a) & the speed of the propagation (Kawamura et al. 2022).

Further studies focused on soft lags at different luminosities (De Marco et al. 2015, 2017) and found that for low accretion rates, the light-travel delay significantly increased to the equivalent of hundreds of gravitational radii. This could suggest the truncation of the accretion disk till these radii. Ever since the launch of NICER the studies of these soft lags have been gaining momentum. Recent studies of the

luminous black hole transient MAXI J1820+070 ([Kara et al. 2019](#); [De Marco et al. 2021](#); [Wang et al. 2021](#)) and compiled NICER observations of other sources ([Wang et al. 2022](#)) found a consistent pattern in the soft lags where they decrease to less than a millisecond during the hard-state rise which then sharply increases to more than ten milliseconds during the transition between the HIMS and SIMS. One explanation that could be given for the sharp rise in the soft "reverberation" lags during the HIMS, when the inner disk radius approaches close to the ISCO, would be if the corona becomes more vertically extended and jet-like ([Kara et al. 2019](#); [De Marco et al. 2021](#); [Wang et al. 2022](#)). This might even be connected to the relativistic jet ejections observed during the state transition according to [Homan et al. \(2020\)](#) and [Wang et al. \(2022\)](#).

As is shown in this section, a lot of progress has been made in studying the hard and soft lags. These lags seem to hold the key to important physical properties of the XRB like the extent & size of the disk and corona as well as the exact geometry of the corona. They also give insight into the accretion states and their origins. Unfortunately, more research has to be done to be able to better understand the origin of the lags between the physical components on the different time scales of variability. The individual previous models are able to explain the different kinds of lags separately. However, when trying to combine them together the models fail to properly explain the observed phenomena.

The problem with Comptonisation delay models is that they require an extremely extended (thousands of gravitational radii) coronae in the hard state. However, this is inconsistent with the reverberation delays that arise from the soft lags. Meanwhile, large PL-disk lags that are observed at low frequencies would only further increase this inconsistency if they correspond to the light-travel delays between the seed photons from the disk and the corona ([Uttley et al. 2011](#)).

The models that use the propagations of accretion fluctuations through a hot flow to explain the low-frequency PL-disk lags seem to clash with the models that explain the hard lags over the same frequency range with the hot-flow propagation.



1.9 Thesis overview

In the previous sections (chapter 1), the importance of these lags has been explained. Their link to constraining the size and extent of the disk & corona as well as its geometry. Which in turn tells us something about the physics behind the variabilities in XRBs and their emissions.

Chapter 2 will be going into the details of a new model made by [Uttley & Malzac \(????\)](#) which combines the previous models and tries to put restraints on the corona while explaining both the hard and soft lags at the same time. It will go into the coding details of the model as well as some of the maths behind it. It will also mention some of the improvements to the original model that have been made.

Once this has been explained chapter ?? will show the results of these improvements will also be announced along with their effects on the total run time. As well as some fitting results that were found using the improved model.

Finally, chapter ?? contains the discussion and conclusion of this thesis.

Chapter 2

Model

As mentioned in section 1.8 the models created in recent years to explain the variabilities and lags in the emissions of X-ray black hole binaries have somewhat lacked the ability to explain multiple components of the hard and soft lags observed. Recently a new model by [Uttley & Malzac \(????\)](#) has appeared to try and simultaneously model multiple components of the previous models while trying to put constraints on the extent and size of the disk and corona as well as the geometry of the corona. They propose a propagation fluctuations model for the lags that would give both the disk-PL hard lags at low frequencies as well as the soft lags at high frequencies. They also link the lags to the coronal geometry to explain the observed lag evolution. Following from their model they show that while accounting for variations of the seed photons that can illuminate the corona as mass accretion fluctuations propagate through the disk to the corona, the observed features naturally show up. As the fluctuations move inward the seed photons are modulated before the corona is heated by them. This causes the corona to first cool and heat after a large viscous time-scale delay. This allows for the production of large hard PL lags even when the corona is small as well as radii in the inner disk.

They believe that if the seed photon variations, the switch to negative, is accounted for, the soft lags are caused by the reverberation. As the fluctuations propagate through the inner regions of the disk, this reverberation causes a slow rise in seed photons. The negative PL-disk lags as well as the hard PL lag would increase as a result of a change in coronal geometry. A vertically extended corona would respond to the seed variations from further out in the disk, causing larger lags. The lags that are predicted by their model would link both the soft and hard lags to the propagation delays instead of the light-travel times. Inferring that the corona would be more compact than those implied by the reverberation light-travel delay and Comptonization models. However, the change in coronal geometry as the system changes states, remains similar.

2.1 Effects of Corona emissions

To be able to model the variation of a quantity $f(t)$ as it responds to a signal perturbation $s(t)$, a so-called impulse response function $g(\tau)$ that helps describe the perturbation in $f(t)$ as a convolution between the signal perturbation and the impulse response. Where this perturbation to $f(t)$ would look as follows, $\delta f(t) = \int_{-\infty}^{\infty} s(t - \tau) * g(\tau) d\tau$, where τ is the time delay and the rest is as mentioned above. In the paper, they use something called the photon index. This allows for the luminosities of the heating and cooling of the corona to the amount of photon flux density variation depending on the time and energy. For this, they assume that the Comptonizing corona is in thermal equilibrium. The cooling of the corona happens through the inverse Compton scattering of seed photons from the black body emitting disk at luminosity L_s . Meanwhile, the corona is heated via an unknown heating mechanism, heating the corona at a luminosity L_h . If these luminosities can be taken as a time series a spontaneous photon index Γ can be constructed to be related to the ratio of the seed photons to the heating photons,

$$\Gamma(t) = \Gamma_0 \left(\frac{L_s(t)}{L_h(t)} \right)^{\beta}, \quad (2.1)$$

where Γ_0 is the photon index for equal heating and cooling luminosities and β is a parameter that describes the change in this ratio in a Comptonizing medium. It depends on the optical depth and temperature of the corona varying from 0 to 1, where at 0 it is insensitive to the heating and seed photons while at 1 it is very sensitive (Pietrini & Krolik 1995; Beloborodov 2001).

The most important part about the model however is the direction of the reaction. Not the precise relation between the photon index and the ratio for the heating vs seed luminosities, but rather what sets the sign of the lags. They believe that the correlation between the photon index and the ratio being positive is a natural occurrence because of the conservation of total luminosity and photon number in the corona. The thermal equilibrium assumption can only be used if the heating and cooling time scales within the corona are small when compared to the variability time scales of the luminosities. The relatively compact corona considered in their model should make sure of that.

[Uttley & Malzac \(????\)](#) uses the following approximation for the photon flux density variation. They take the seed photons to be monochromatic with the energy E_s , this makes the total number of photons L_s/E_s . Under the assumption that the total number of photons is conserved during the process of Comptonization and the cut-off photon energy is E_{cut} is much greater than E_s , the photon flux density variation can be constructed as follows,

$$N(E, t) = \frac{L_s(t)(\Gamma(t) - 1)}{E_s^2} \left(\frac{E}{E_s} \right)^{-\Gamma(t)}, \quad (2.2)$$

where $N(E, t)$ is this photon flux density, L_s is the seed photon luminosity and Γ is the photon index.

When assuming the perturbations are small, the equations 2.1 and 2.2 can be linearized and they find the following functions for impulse responses for the photon index and the photon flux density,

$$g_\Gamma(\tau) = \langle \Gamma \rangle \beta \left(\frac{g_s(\tau)}{\langle L_s \rangle} - \frac{g_h(\tau)}{\langle L_h \rangle} \right), \quad (2.3)$$

$$g_{pl}(E, \tau) = \langle N(E) \rangle \left([1 - u(E)] \frac{g_s(\tau)}{\langle L_s \rangle} + u(E) \frac{g_h(\tau)}{\langle L_h \rangle} \right), \quad (2.4)$$

where $\langle A \rangle$ is the average of A over time and A is anything that is perturbed by the changes in the seed and heating luminosities. Which in this case are the luminosities, photon index, and photon flux index. The impulse responses for the seed and heating g_s & g_h are all dependent on the physical system producing the variation in the luminosities. $u(E)$ is the energy dependence of equation 2.4 and is defined as follows,

$$u(E) = \beta \langle \Gamma \rangle \left(\ln \left(\frac{E}{E_s} \right) - \frac{1}{\langle \Gamma \rangle - 1} \right), \quad (2.5)$$

it gives the energy-dependent impulse response shape of the photon flux density impulse response. It takes into account the seed and heating impulse responses according to the energy of the PL photons that are looked at. $u(E)$ looks at the pivoting of the power-law spectrum around a pivoting energy E_{piv} where $g_{pl}(E_{piv}, \tau) = 0$.

Chapter 3

Results

3.1 Tests

[1](#)

3.2 Fits

[2](#)

¹Comment: Text about the tests and stuff come here

²Comment: Describe target + fitting parameters + maybe the explanation of what is happening?
Although that is technically already mentioned in section [1.8](#) & [2](#)

³Comment: Do I also have to put in the grid size of the fit as well as the other default fitting parameters in the figure caption or only in the text or a table?

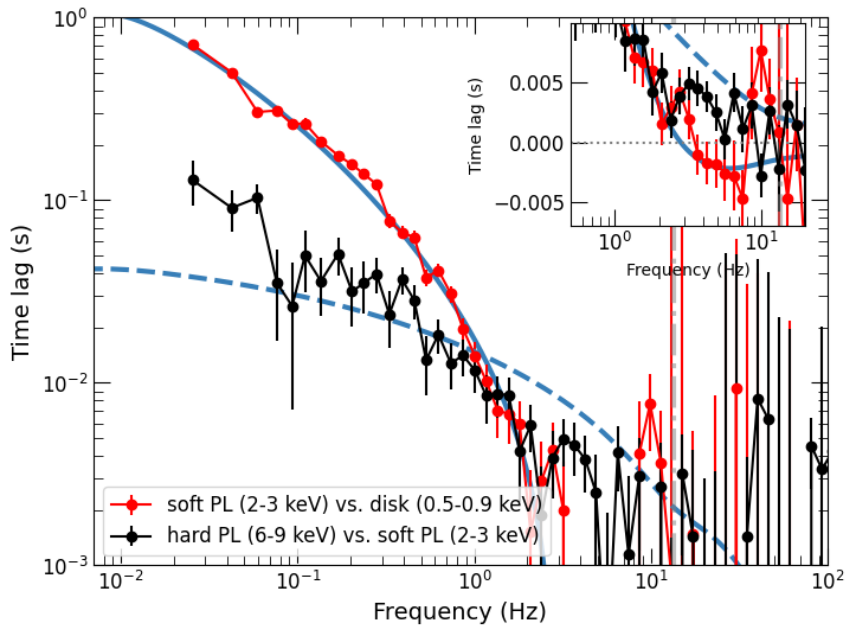


FIG. 3.1 – This figure shows the resulting fit from the C++ model for the XMM-Newton data of GX 399-4 in the hard state taken with XMM's EPIC-pn instrument [Uttley et al. \(2011\)](#). It shows the data for the time lags between the Soft PL energy band and the disk energy band in red. In blue is the fit shown for these soft lags. It also shows the time lags between the soft and hard PL energy bands. In dashed blue is the fit shown for these hard lags.³

Chapter 4

Conclusion

Bibliography

- Abbott, R., Abbott, T. D., Abraham, S., et al. 2020, Phys. Rev. Lett., 125, 101102
- Altamirano, D. & Méndez, M. 2015, MNRAS, 449, 4027
- Arévalo, P. & Uttley, P. 2006, MNRAS, 367, 801
- Balbus, S. A. & Hawley, J. F. 1991, ApJ, 376, 214
- Balbus, S. A. & Hawley, J. F. 1992, ApJ, 400, 610
- Balbus, S. A. & Hawley, J. F. 1998, Reviews of Modern Physics, 70, 1
- Bambi, C. 2021, arXiv e-prints, arXiv:2106.04084
- Begelman, M. C., Armitage, P. J., & Reynolds, C. S. 2015, ApJ, 809, 118
- Belloni, T. M. & Motta, S. E. 2016, in Astrophysics and Space Science Library, Vol. 440, Astrophysics of Black Holes: From Fundamental Aspects to Latest Developments, ed. C. Bambi, 61
- Beloborodov, A. M. 2001, Advances in Space Research, 28, 411
- Bolton, C. T. 1972, Nature, 235, 271
- Boss, A. P. & Keiser, S. A. 2014, ApJ, 794, 44
- Braes, L. L. E. & Miley, G. K. 1971, Nature, 232, 246
- Bright, J. S., Fender, R. P., Motta, S. E., et al. 2020, Nature Astronomy, 4, 697
- Celotti, A., Miller, J. C., & Sciama, D. W. 1999, Classical and Quantum Gravity, 16, A3
- Colbert, E. J. M. & Mushotzky, R. F. 1999, ApJ, 519, 89
- De Marco, B., Ponti, G., Muñoz-Darias, T., & Nandra, K. 2015, ApJ, 814, 50
- De Marco, B., Ponti, G., Petrucci, P. O., et al. 2017, MNRAS, 471, 1475

- De Marco, B., Zdziarski, A. A., Ponti, G., et al. 2021, *A&A*, 654, A14
- Dhawan, V., Mirabel, I. F., & Rodríguez, L. F. 2000, *ApJ*, 543, 373
- Done, C., Gierliński, M., & Kubota, A. 2007, *A&A Rev.*, 15, 1
- Dubus, G., Kim, R. S. J., Menou, K., Szkody, P., & Bowen, D. V. 2001, *ApJ*, 553, 307
- Fender, R. P., Belloni, T. M., & Gallo, E. 2004, *MNRAS*, 355, 1105
- Fender, R. P., Homan, J., & Belloni, T. M. 2009, *MNRAS*, 396, 1370
- Finkelstein, D. 1958, *Physical Review*, 110, 965
- Frank, J., King, A., & Raine, D. J. 2002, *Accretion Power in Astrophysics: Third Edition*
- Gendreau, K. C., Arzoumanian, Z., & Okajima, T. 2012, in Society of Photo-Optical Instrumentation Engineers (SPIE) Conference Series, Vol. 8443, Space Telescopes and Instrumentation 2012: Ultraviolet to Gamma Ray, ed. T. Takahashi, S. S. Murray, & J.-W. A. den Herder, 844313
- Giacconi, R., Gursky, H., Paolini, F. R., & Rossi, B. B. 1962, *Phys. Rev. Lett.*, 9, 439
- Giannios, D., Kylafis, N. D., & Psaltis, D. 2004, *A&A*, 425, 163
- Gierliński, M., Zdziarski, A. A., Poutanen, J., et al. 1999, *MNRAS*, 309, 496
- Grinberg, V., Pottschmidt, K., Böck, M., et al. 2014, *A&A*, 565, A1
- Hawley, J. F. & Balbus, S. A. 1991, *ApJ*, 376, 223
- Hawley, J. F. & Balbus, S. A. 1992, in American Astronomical Society Meeting Abstracts, Vol. 181, American Astronomical Society Meeting Abstracts, 71.05
- Hewish, A., Bell, S. J., Pilkington, J. D. H., Scott, P. F., & Collins, R. A. 1968, *Nature*, 217, 709
- Höfner, S., Gautschy-Loidl, R., Aringer, B., & Jørgensen, U. G. 2003, *A&A*, 399, 589
- Homan, J., Bright, J., Motta, S. E., et al. 2020, *ApJ*, 891, L29
- Kalemci, E., Dinçer, T., Tomsick, J. A., et al. 2013, *ApJ*, 779, 95
- Kara, E., Steiner, J. F., Fabian, A. C., et al. 2019, *Nature*, 565, 198
- Kawamura, T., Axelsson, M., Done, C., & Takahashi, T. 2022, *MNRAS*, 511, 536
- Koljonen, K. I. I. & Russell, D. M. 2019, *ApJ*, 871, 26

Bibliography

- Kormendy, J. & Richstone, D. 1995, ARA&A, 33, 581
- Kotov, O., Churazov, E., & Gilfanov, M. 2001, MNRAS, 327, 799
- Kristian, J., Brucato, R., Visvanathan, N., Lanning, H., & Sandage, A. 1971, ApJ, 168, L91
- Kylafis, N. D., Papadakis, I. E., Reig, P., Giannios, D., & Pooley, G. G. 2008, A&A, 489, 481
- Lyubarskii, Y. E. 1997, MNRAS, 292, 679
- Mahmoud, R. D. & Done, C. 2018a, MNRAS, 480, 4040
- Mahmoud, R. D. & Done, C. 2018b, MNRAS, 473, 2084
- Mahmoud, R. D., Done, C., & De Marco, B. 2019, MNRAS, 486, 2137
- Markoff, S., Nowak, M. A., & Wilms, J. 2005, ApJ, 635, 1203
- Mastroserio, G., Ingram, A., & van der Klis, M. 2018, MNRAS, 475, 4027
- Mattsson, L. & Höfner, S. 2011, A&A, 533, A42
- Miller-Jones, J. C. A., Sivakoff, G. R., Altamirano, D., et al. 2012, MNRAS, 421, 468
- Miyamoto, S., Kitamoto, S., Mitsuda, K., & Dotani, T. 1988, Nature, 336, 450
- Nowak, M. A., Wilms, J., & Dove, J. B. 1999, ApJ, 517, 355
- Pietrini, P. & Krolik, J. H. 1995, ApJ, 447, 526
- Podsiadlowski, P., Rappaport, S., & Pfahl, E. D. 2002, ApJ, 565, 1107
- Rapisarda, S., Ingram, A., Kalamkar, M., & van der Klis, M. 2016, MNRAS, 462, 4078
- Reig, P., Kylafis, N. D., & Giannios, D. 2003, A&A, 403, L15
- Rothschild, R. E., Boldt, E. A., Holt, S. S., & Serlemitsos, P. J. 1974, ApJ, 189, L13
- Sandin, C. & Höfner, S. 2003, A&A, 404, 789
- Sandin, C. & Höfner, S. 2004, A&A, 413, 789
- Schwarzschild, K. 1916, Sitzungsberichte der Königlich Preußischen Akademie der Wissenschaften, 189
- Shakura, N. I. & Sunyaev, R. A. 1973, A&A, 24, 337
- Shapiro, S. L., Lightman, A. P., & Eardley, D. M. 1976, ApJ, 204, 187

- Shipman, H. L. 1975, *Astrophys. Lett.*, 16, 9
- Strüder, L., Briel, U., Dennerl, K., et al. 2001, *A&A*, 365, L18
- Tauris, T. M., van den Heuvel, E. P. J., & Savonije, G. J. 2000, *ApJ*, 530, L93
- Turner, M. J. L., Abbey, A., Arnaud, M., et al. 2001, *A&A*, 365, L27
- Uttley, P., Cackett, E. M., Fabian, A. C., Kara, E., & Wilkins, D. R. 2014, *A&A Rev.*, 22, 72
- Uttley, P. & Malzac, J. ?????
- Uttley, P., McHardy, I. M., & Vaughan, S. 2005, *MNRAS*, 359, 345
- Uttley, P., Wilkinson, T., Cassatella, P., et al. 2011, *MNRAS*, 414, L60
- Wang, J., Kara, E., Lucchini, M., et al. 2022, *ApJ*, 930, 18
- Wang, J., Mastroserio, G., Kara, E., et al. 2021, *ApJ*, 910, L3
- Webster, B. L. & Murdin, P. 1972, *Nature*, 235, 37
- Wilkinson, T. & Uttley, P. 2009, *MNRAS*, 397, 666
- Wilson, A. 2005, *ESA achievements : more than thirty years of pioneering space activity*, 3rd edn., *ESA BR* (ESA Publications)
- Zdziarski, A. A., Dziełak, M. A., De Marco, B., Szanecki, M., & Niedźwiecki, A. 2021, *ApJ*, 909, L9

Appendix A

Code

[1](#)

¹Comment: Not sure if I should also include the C++ code here. And if so also the Python code. For the explanation of what I have done, I should probably either put the code bits or just put all the code in the appendix... Not sure if that maybe is too much for in the appendix. Maybe it is better to have it via Github...